Lifetime testing of a flexure based natural gas fired 1 kW thermoacoustic genset

Thomas W. Steiner[*], *M. Hoy, K. B. Antonelli, M. Malekian, G. D. S. Archibald, T. Kanemaru, W. Aitchison, B. De Chardon, K. T. Gottfried, M. Elferink, T. Henthorne, B. O'Rourke, and P. Kostka*

Etalim Inc. 3718 Triumph St. Burnaby, BC, Canada

Abstract. Etalim has developed and lifetime tested a flexure-based thermoacoustic (TAC) genset operating at high pressure and frequency. It is an efficient and practical 1 kWe genset ready for deployment as a genset or a micro-cogeneration system when integrated with a recuperated natural gas burner and stroke controlling power electronics. It is a maintenance-free, extreme reliability genset particularly suited for remote power applications. The genset is fully costed and designed for manufacturing. Fuel-to-electric efficiency of 22% has been achieved, and one remaining avenue for significant improvement identified. A test TAC has been run for a cumulative time of about 8000 hours to date without any component failures.

1 Introduction

Etalim has been building flexure-based engines for many years. Some of our previous work has been presented at previous Stirling engine conferences [1,2]. These engines are characterized by high-frequency operation at about 460 Hz and use relatively high pressure (12 MPa) helium working gas. The high frequency and pressure result in good power density despite the limited swept volume allowed with a flexure transducer. The flexure transducers must be mechanically resonant at the operating frequency to be efficient [3]. Resonant operation is achieved using a lightweight but very stiff tube spring, resulting in a transducer linear alternator combination that is 87% efficient at a power output of 1 kW [4].

The engine development has now progressed to the point where we have a production-ready 1 kW electrical output engine. A highly efficient recuperated natural gas burner heats the engine. A circulating fluid with a radiator to ambient cools the engine. Electrical output is provided by a power electronics (PE) module that controls the engine stroke. The result is a load-following genset with a full power fuel-to-electric efficiency of 22%. This

[*] Corresponding author: tsteiner@etalim.com

engine consists of two main modules with an acoustic-to-electric generator module (GM) spatially separated with ducts from the thermal module (TM) acoustic amplifier component.

There are not many reported thermoacoustic engines heated by hot gas in the literature. One example was a lower power density engine without electrical output [5]. Heat transfer through pressure vessel boundaries is particularly challenging in high power density systems with high heat flux densities. Most of the thermoacoustic engines in the literature have avoided this difficult practical problem by using electric cartridge heaters within the pressure vessel. This engine also has higher (24%) heat-to-electrical conversion efficiency than other thermoacoustic engines enumerated in the literature [6,7] by a considerable margin. The inclusion of a 94% efficient recuperated burner in the system for heat delivery results in a fuel-to-electric efficiency of 22%, which is already very competitive with Stirling engines with similar ~1 kW output power capability. There is one clearly identified avenue for further improvement which will raise this efficiency to 27%.

This engine has now been life tested in a combined heat and power (CHP) application for an extended period without any failures. These results, discussed in this paper, should go some way to substantiating our claims that this is an ultra-reliable, minimal maintenance engine that is furthermore mechanically considerably simpler than competing Stirling engines.

2 Apparatus description

A schematic of the thermoacoustic converter (TAC) apparatus is shown in Fig. 1. The main components are the thermal module (TM), the generator module (GM), and the power electronics (PE). The TM has a central bore at ambient pressure into which the recuperating burner is inserted from the top. The fuel/air mixture is introduced at the bottom burner flange. A fan pushes the premix down the counterflow recuperator, where it is heated to about 600 °C by exchanging heat with the exhaust traveling upwards. The mixture is then combusted in the center of the TM. After the combustion chamber, the heat is extracted from the combustion products in a set of tubes embedded in a heat spreader copper core [8]. These tubes contain additional heat exchanger inserts to increase the surface area in contact with the hot flue gasses. Furthermore, these tubes are thin wall Inconel and form part of the pressure vessel. Using a set of tubes in parallel as the pressure vessel wall that conducts the heat, a relatively large conduction area and short conduction path may be achieved through the low conductivity superalloy, thereby minimizing the thermal resistance for external heat input.

A set of six copper heat exchangers of a custom design [9] are brazed to the copper core and match up with six in parallel regenerators disposed in a radial pattern around the hot core [8]. These heat exchangers are unique in that the flocked fiber heat exchange layer is only about 1 mm long in the acoustic flow direction and in that the heat flows in this same direction. The regenerator is split into six parallel smaller regenerators to manage thermal expansion stresses. The regenerators are fabricated from etched foil rolled up into cylinders and diffusion bonded into porous stainless-steel cylinders 30 mm in diameter and 25 mm long [10]. The regenerators have a hydraulic radius of ~19 μm.

On the cold side of the regenerators, distal from the hot core is another set of similar heat exchangers. These are cooled by a circulating fluid that transfers heat to the ambient environment with an external radiator. The cold exchangers are free to move radially outwards and downwards in response to hot core thermal expansion since they are only connected by compliant tubes to the outer TM pressure vessel [8].

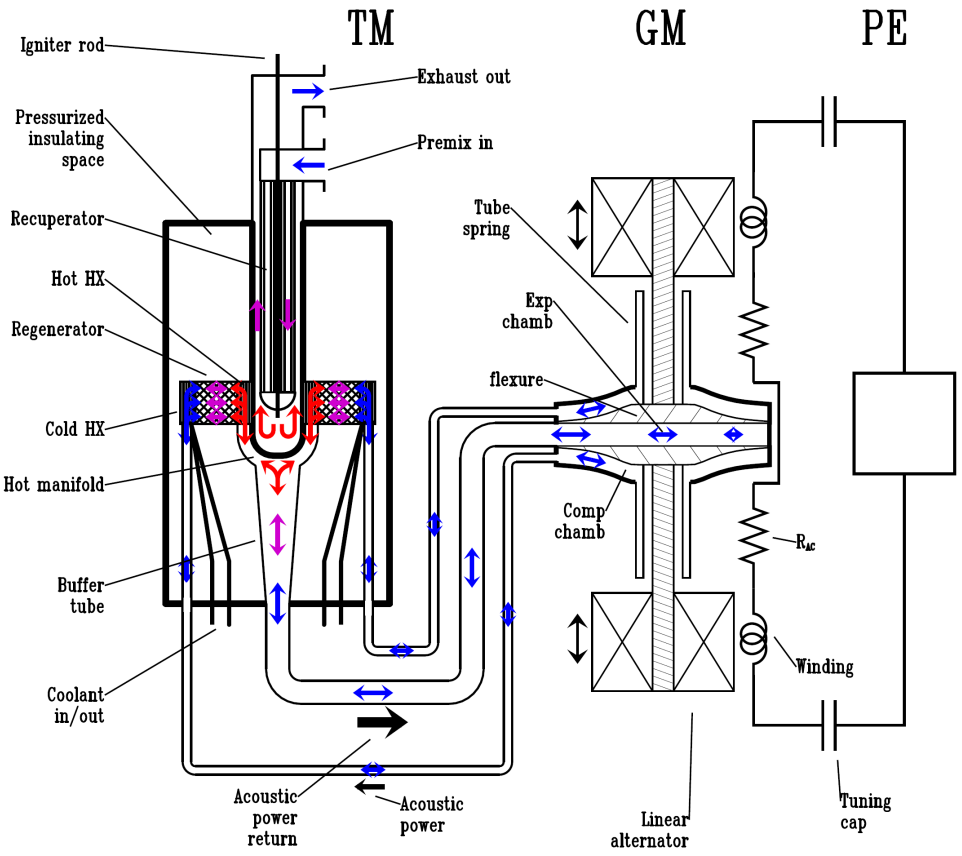

Fig. 1. Schematic of the apparatus showing the three main modules. The thermal module (TM), the generator module (GM), and the power electronics (PE). Colour coded by temperature, the double-headed arrows show the oscillating helium flows at several locations in the apparatus. The colour-coded single-headed arrows indicate the cold fuel/air mixture entering the TM, preheated in the recuperator, and the exhaust after combustion cooled back close to ambient before exiting the burner. The GM linear alternators vibrate with an amplitude of about 350 µm and provide the electrical input to the PE.

Acoustic power created by the flexure motion in the compression chamber travels from the GM in a set of parallel transmission ducts and is fed to the cold side of the regenerators. The regenerator's thermal gradient causes the working gas carrying the acoustic power to undergo a Stirling cycle, amplifying this acoustic power [11,12]. The amplified acoustic power exiting the hot sides of the regenerators is collected in a hot manifold. The accumulated acoustic power then travels down a slightly tapered buffer tube in the bottom half of the TM and exits the TM. The buffer tube allows the working gas temperature to drop back to ambient without significant loss of power since, unlike in the regenerator, the thermal contact is minimal in this open duct. The duct is slightly tapered to suppress convection [13]. The amplified acoustic power is then transported back to the GM in a single larger diameter duct where the motion of the flexures in the expansion chamber absorbs it. The extra acoustic power over what is needed to restart the cycle on the compression side is extracted by the linear alternators and converted to electricity. The GM

is a dual opposed design with a single shared expansion chamber to allow for substantial vibration cancellation.

Note that the flexure motion amplitude in the GM is only 200 μm. The tube spring provides the primary spring to allow mechanical resonance at the design operating frequency of 460 Hz. These springs work by pure axial compression and extension of thin-wall tubes. The tube springs and the diaphragm flexures are the components subject to alternating stress during operation and must be designed accordingly. The GM dynamics and performance are discussed in detail elsewhere [4]. They will not be discussed further here except to note that this transducer's full power mechanical-to-electrical conversion efficiency is 87%, which is better than other linear alternator transducers discussed in the literature [3,14].

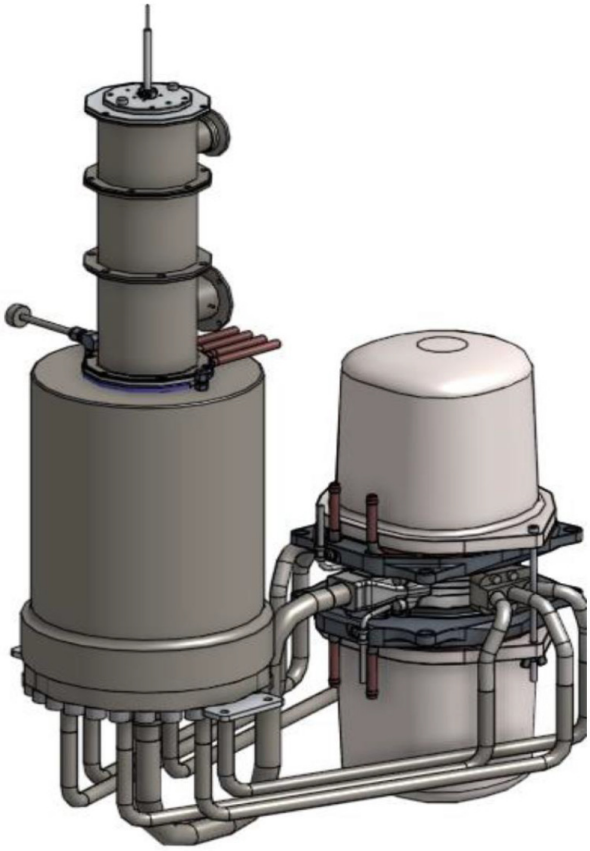

Fig. 2. TAC system. Rendering of the TM with burner inserted on the left and GM on the right. The TM is plumbed to the GM with 6 in parallel 16 mm diameter ducts on the compression side, and the power is returned with a single 25 mm diameter duct on the expansion side.

The linear alternator electrical output from the GM goes to the PE module as in the schematic of Fig. 1. In the schematic, the upper and lower linear alternators are wired in series to double the voltage, but parallel wiring is also possible. Tuning capacitors are needed to cancel the inductance of the windings so that the PE load can function as a purely resistive load [4]. The engine flexure amplitude and thus the power output is implicitly controlled electronically by setting the voltage level of the PE input.

The two linear alternators have been designed and wired to output around 200 Vrms at full stroke, with each side contributing about 500 W. The output voltage and current are near perfect sinewaves at the TAC operating frequency of 460 Hz when the PE presents a purely resistive load. Several different PEs are possible. We have built custom circuitry that converts the 460 Hz AC output from the GM to 24 V DC. This circuit also sets the input voltage so that power delivered from the TAC matches the power demand at 24V and thus turns the TAC into a load-following genset. In this operational mode, suitable for use as a remote power genset, the heating power follows the load power indirectly using a simple temperature servo. The hot core temperature is kept close to the setpoint by adjusting the fuel and air flows and will thus change the heating power to keep the temperature constant.

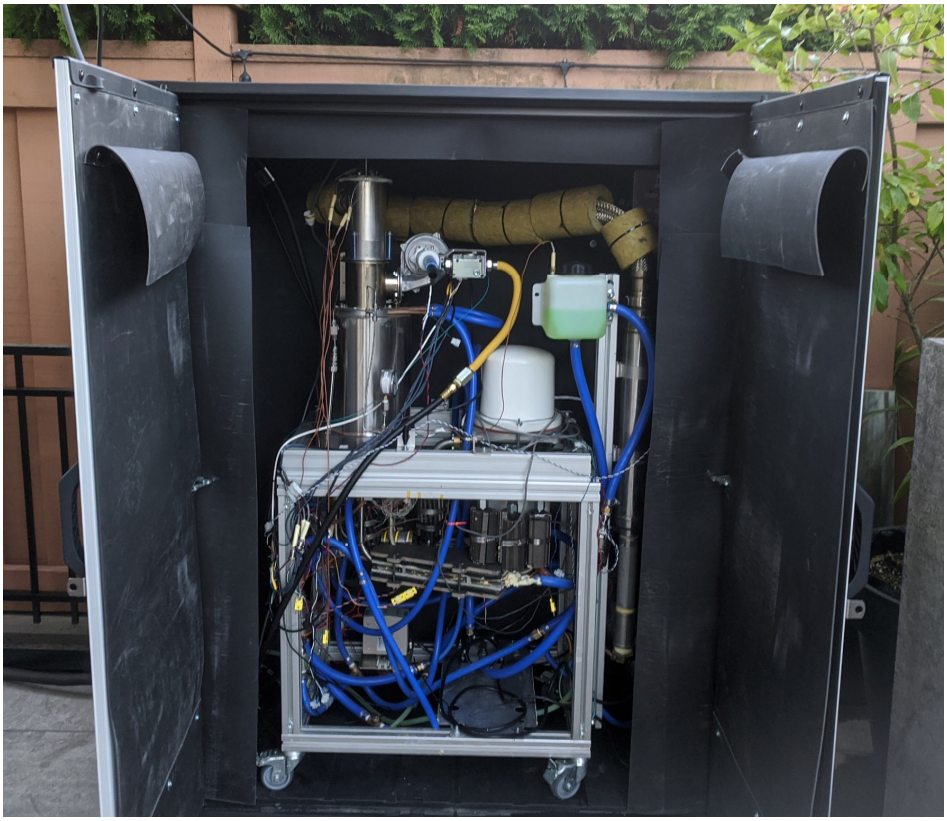

Fig. 3. A picture of a TAC installed in a garden shed and used in combined heat and power (CHP) mode to heat a house. See https://youtu.be/t28hXxKnF-A . The total runtime to date is ~8000 hours.

We have also run the output of the TAC through a bridge rectifier and into a solar grid-tie inverter running in constant voltage mode when the TAC was configured for CHP home heating, as shown in Fig. 3. The grid-tie inverter used in this instance did not have an extensive input voltage adjustment range. Thus, the TAC output was adjusted by adjusting the hot core setpoint temperature instead of the load voltage for this application test. This meant that the TAC ran near full mechanical stroke for the duration even as the output power was reduced by reducing the core temperature. Changing the core temperature instead of the flexure amplitude is an alternate but slow means of modulating the TAC output.

Another near-constant voltage load is a battery bank wired to match the full stroke rectified output voltage of the TAC. We have run successful direct battery charging experiments with a PE consisting only of a bridge rectifier and the battery bank. In this application, the core temperature may be ramped down to slowly reduce the charging current as the battery nears full charge.

3 Simulation model

This engine and our earlier engines [1,2] may be modelled using thermoacoustic theory [11,12]. The method used was a one-dimensional integration of the acoustic propagation in the acoustic power flow direction starting in the compression chamber of the GM and ending in the expansion chamber of the GM. The TAC is modelled using 43 distinct segments, with each segment corresponding to a part of the TAC with a particular flow geometry or other characteristics. Our simulation method is like what is used by the freely available, general-purpose, thermoacoustic modelling software DELTAE [12] but customizations [15] are needed to model the TAC's flexure transducer with flows substantially parallel to the flexure surfaces rather than perpendicular. Thus, we have used our proprietary simulation software using the same underlying mathematics and principles.

Helium was chosen as the working gas since operation at high frequency is necessary to provide good power density given the limited stroke of the flexure diaphragms. At the frequencies used, helium has a wavelength of about 2 m which is convenient for plumbing together the TM and GM with ducts ~1 m long. System simulation results show equally good results using hydrogen with somewhat longer ducts. However, helium and hydrogen simulation results are substantially better than simulation results, ignoring the layout constraints, using nitrogen or argon with much shorter ducts.

In Fig. 4, one set of experimental results that demonstrates the load following ability of the TAC is shown. The solid lines are the thermoacoustic simulation results and match the experimental measurements reasonably well, indicating that our model can provide useful predictions of engine performance and design guidance. The comparison of the performance of this TAC to our thermoacoustic model as functions diaphragm amplitude and of hot and cold side temperatures is discussed in detail elsewhere [15] and will not be repeated here.

4 Measured performance

Peak output at the design diaphragm flexure amplitude of 200 µm is seen to be just over 1 kW in Fig. 4 with a heat-to-electric conversion efficiency of 24 %. This flexure amplitude corresponds to about 350 µm linear alternator amplitude due to the stretch of the connecting rod [4]. As discussed above, the flexure amplitude was controlled by setting the input voltage of the PE. Output power scales with the flexure amplitude, and more power would be available by increasing the flexure amplitude beyond the nominal maximum, which may be done for short durations without impacting the flexure lifetime significantly. Efficiency reaches a peak near the nominal maximum flexure amplitude as intended by design.

Increasing the amplitude further would lead to marginally lower efficiencies as the non-linear losses become a more significant fraction of the total losses. Also, the regenerator temperature gradient is reduced due to larger heat conduction temperature deltas in the heat exchangers as more heat is transferred at higher power.

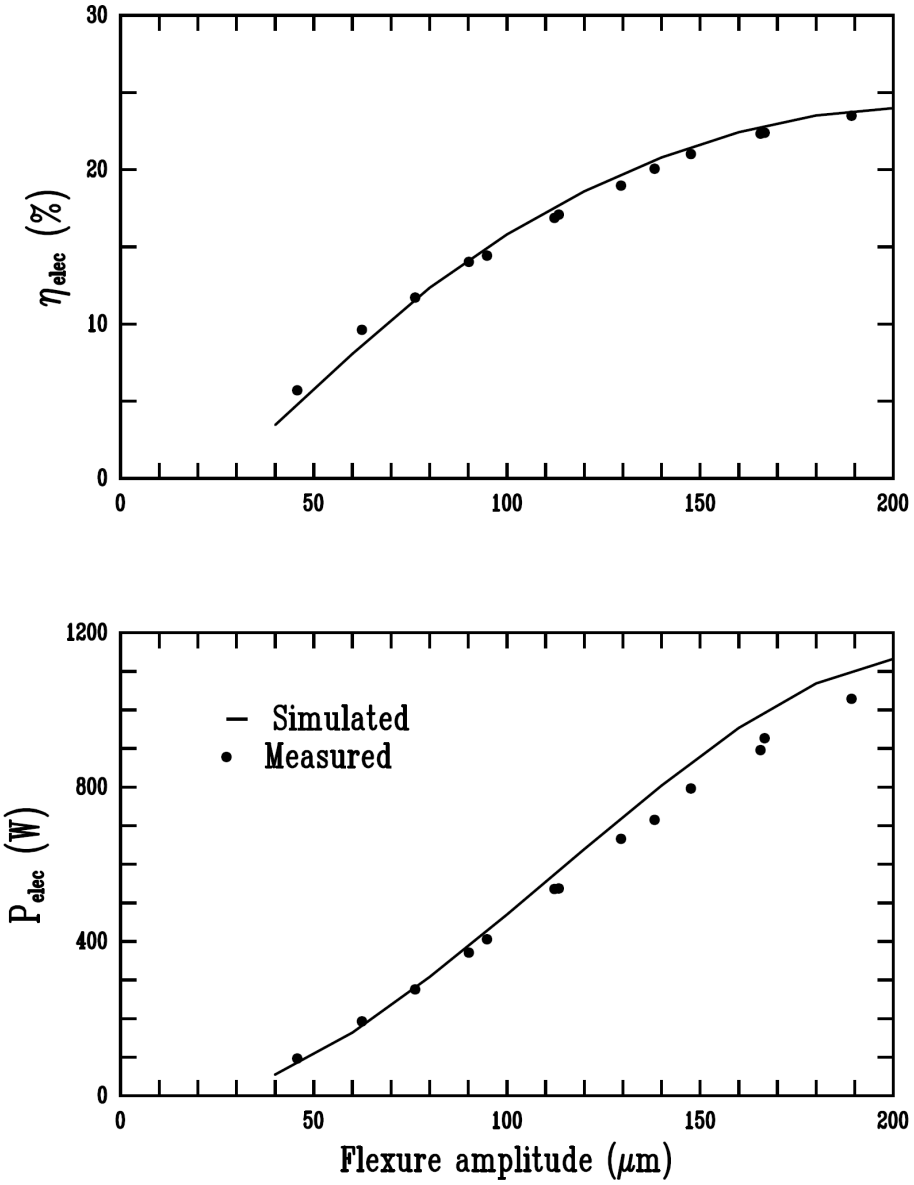

Fig. 4. Measured and simulated TAC performance as a function of flexure amplitude with the hot core heated to 700 °C and coolant at 26 °C.

Efficiency decreases as the flexure amplitudes are reduced, despite lower non-linear losses and temperature deltas because of the parasitic overhead heat transfer from the hot to the cold side of 1.2 kW (as measured) at a hot core temperature of 700 °C. This overhead amount is about 500 W greater than initially anticipated from the design and constitutes the only significant deviation of the as-built apparatus from the design goals. The cause of this extra overhead heat transfer was determined to be unwanted convection within the TM, as evidenced by the dependence on the working gas type and pressure. Outside of the working volume but inside the TM pressure vessel, the TM is charged to the same mean

pressure as the working gas. Despite this volume being filled with microporous insulation, we have not succeeded in sufficiently suppressing convection in this volume to bring down the overhead heat transfer to a pure conduction amount. It is much more difficult to stop the high-pressure helium convection than was anticipated, and none of the rework attempts succeeded in reducing convection to negligible levels. This unwanted heat transfer is very detrimental to the overall TAC efficiency as every 100 W of extra heat transfer overhead corresponds to about 1% system efficiency loss. The TAC would thus be 27% instead of 22% fuel-to-electric efficient had we achieved the design goals.

The fuel used was natural gas with a composition of 91% methane, 6% ethane, 2% propane and 1% trace components. The fuel input was measured using a Sierra Instruments mass flow sensor calibrated for methane but with a correction applied for the natural gas composition. The fuel energy content was also determined from the composition and used to calculate the fuel energy input. When configured for use as a CHP device, the exhaust is further cooled after the burner by a condenser to extract the water heat of condensation from the exhaust stream. The condenser is visible on the far right of the apparatus in Fig. 3. The coolant used for the results in Fig. 4 was water with the coolant flow and temperatures measured using a pair of IFM flow and temperature sensors. The TAC heat output was calculated from the flow rate and the water temperature difference. For the peak electrical output of 1030 W in Fig. 4, the lower heating value (LHV) power input from the fuel was 4640 W for a fuel-to-electric conversion efficiency of 22%. The heat output was ~3500 W. The total efficiency measured was thus ~98% using the LHV fuel energy or ~89% using the higher heating value (HHV).

A new TM design that does not use high-pressure gas in the insulating volume has now been proven. However, a complete engine based on this new TM design is not yet at the same technology readiness level (TRL) as the TAC reported on here, to which we assign a TRL of 7. Furthermore, the new TM design is modular and lower cost and will provide additional advantages in addition to the 27% fuel-to-electrical conversion efficiency once completed.

5 Life testing

One TAC has been lifetime tested for a cumulative ~8000 hours to date, as shown in Fig. 5 (first several hundred hours not logged). The cumulative data consists of several experiments with the first ~3000 hours run at constant hot core temperature but variable cold side temperature and occasionally a flexure stroke larger or smaller than the nominal maximum. The last ~5000 hours consist of testing the same TAC in a CHP mode where the PE input voltage was fixed at 190 V by a grid-tie inverter resulting in a near-constant flexure stroke slightly less than the nominal maximum. Due to this grid-tie inverter's limited input voltage adjustment range (190 V was the minimum), the TAC output in this CHP mode was modulated to match the heating demand by adjusting the hot side temperature instead of the flexure amplitude. Thus, this TAC has run near full flexure amplitude for almost the entire 8000 hours.

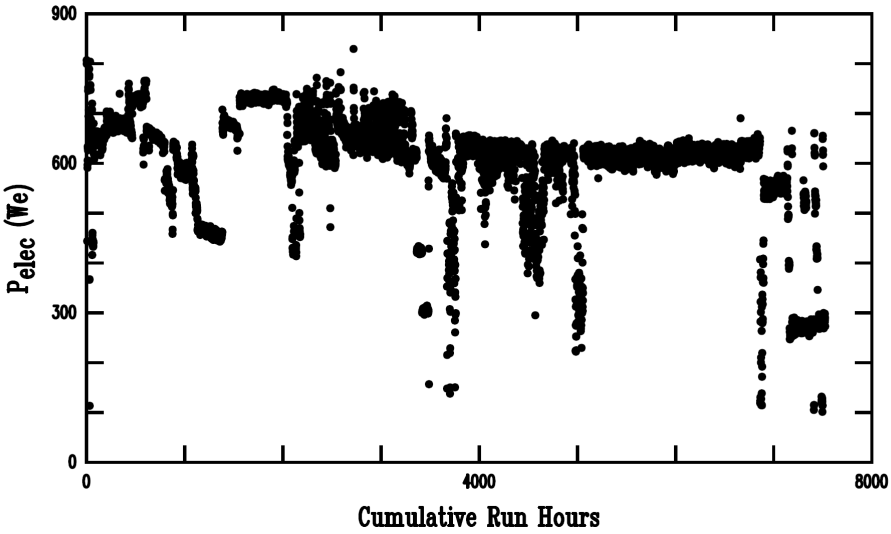

Fig. 5. Cumulative run time of the CHP TAC. Note that the output power was deliberately modulated down at times to match the house heat demand by changing the core temperature rather than the flexure stroke. Only the last ~5000 hours correspond to the CHP test. The first 3000 hours were different experiments with, at times, different flexure amplitudes and lower coolant temperature but with constant hot core temperature.

This particular TAC was the first built instance of this design and, due to a GM defect, needed to be run at 420 Hz rather than the 460 Hz of later versions. This first instance also had lower quality early regenerators with higher than nominal flow resistance values. Thus, this particular TAC instance is less powerful and less efficient than the later TAC used for the experimental results of Fig. 4. Nevertheless, the first instance was chosen for continued lifetime testing, even when newer TACs became available due to the already accumulated run hours. The primary purpose of the lifetime test was to prove that the components subject to alternating stress, namely the tube spring and the diaphragm flexures, can survive long enough to make a commercial product.

At the ~420 Hz operating frequency of this particular TAC, the 8000 operating hours correspond to 1.2×10^{10} flexure cycles. This is far into the gigacycle regime, and fatigue failure with continued running under these same conditions is very unlikely. The reliability of the components subject to alternating stresses has thus been demonstrated.

We have also done accelerated life testing of tube spring coupons by overstressing these coupons and comparing the measured fatigue failure results to published fatigue data [16] on the 15-5 precipitation hardening stainless steel used for the parts in the GM subject to alternating stress. The results of the accelerated lifetime testing are shown in Fig. 6. The coupons were run at approximately double the design stress (thus corresponding to double the nominal maximum flexure amplitude) to failure, which occurred between 10^7 and 10^8 cycles. The known 15-5 fatigue curve was shifted down slightly to match the mean of the test coupons. This shift is consistent with a small surface finish derating, or else it may be compensating for minor sensor calibration errors. The open diamond's y-axis position corresponds to the design peak alternating stress of 240 MPa in these components. The diamond's x-axis position corresponds to the cycles accumulated in the lifetime testing of the CHP TAC to date.

The reference curve for 15-5 only extends to 10^9 cycles. While 15-5 does not reach an actual endurance limit, allowed stress only drops 5-10% per decade in the gigacycle regime [17]. The published data is thus extended out to 10^{12} cycles with the same slope in Fig 6. This many cycles at the operating frequency of the TAC would correspond to 70 years of continuous operation. The peak design stress of the components used in the TAC is well below the extrapolated material failure stress at 10^{12} cycles. No fatigue failure is thus expected for the life duration in any practical TAC application, provided there are no manufacturing defects in the components. Any manufacturing defects will tend to produce a very early failure. The substantial margin can accommodate minor manufacturing deviations in component dimensions. The margin also allows for some short duration over stroke events without significant effects on expected fatigue life.

Another possible failure mode is working gas leakage, as helium is notoriously difficult to contain. However, helium does not diffuse through metals and thus, provided there are no polymer seals and no pinhole leaks, helium can be contained indefinitely. The TAC, as designed for volume manufacturing, may be fabricated without any polymer seals. The CHP TAC, as tested, still has some polymer seals. Nevertheless, no appreciable helium working gas leakage was observed over many months of operation.

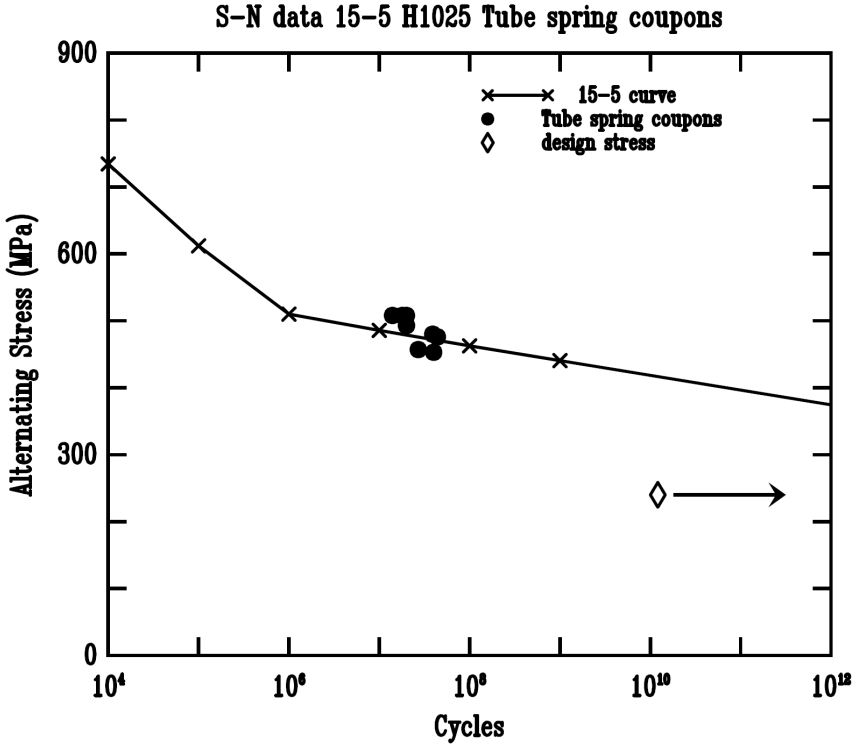

Fig. 6. Accelerated fatigue test of tube spring coupons to failure. Open diamond corresponds to the peak design stress of the components subject to alternating stress and the number of cycles accumulated by the CHP test TAC to date.

Creep of the hot pressure vessel walls is a further potential lifetime concern. The hot pressure vessel walls consist of a set of Inconel exhaust gas tubes extending through the central copper core of the TM. These are made as thin-walled as possible to provide the lowest thermal resistance for heat conduction through the pressure vessel walls. Creep resistance is an exponential function of temperature, so knowledge of the temperature

distribution is a crucial design input. Non-linear FEA creep analysis of the entire hot core was done with temperature input from a thermal FEA model. As designed, the engine may be operated at a copper core temperature of 700 °C without exceeding 1% creep of the Inconel hot core even for long-term (7 years) continuous operation. As a 1% creep does not constitute failure, practical lifetimes are likely much longer. As creep has exponential temperature dependence, substantially longer life may be obtained with a very modest decrease in core operating temperature. At the nominal operating temperature of 700 °C, the time scales at the design stresses are years. Thus, short-duration over-temperature events are not catastrophic as the material strength remains far above the pressure-induced stresses.

6 Comparison to Stirling engines

Unlike Stirling engines, the TAC does not have any sliding or rotating parts. Since no displacer is needed, it conceptually has only one barely moving part. It is almost like a solid-state heat to electricity converter while still producing mechanical power efficiently with the Stirling cycle. Extreme reliability is achieved at a lower cost since no tight tolerance clearance seals are required. The actual TAC as-built uses a back-to-back GM so that there are then two barely moving parts to achieve vibration balance. The TAC produces minimal vibration as compared to a free-piston Stirling engine. Any residual vibration is furthermore at an order of magnitude higher frequency and thus is much easier to attenuate. Splitting of the machine into separate thermal acoustic amplification and acoustic-to-electrical conversion modules provides greater heat input flexibility than can be achieved with Stirling engines. The waste heat recovery version of the TAC [18] provides an example of this flexibility.

Despite the minimal residual vibration, the high-frequency operation results in an acoustically loud device given the human ear's response. Still, a TAC may be made as quiet as necessary for any application by enclosing it in one or more enclosures. Placed in a plastic garden shed (Fig. 3), the TAC external sound level is about 70 dBa.

Another disadvantage of the TAC is that the acoustic tuning is dependent on the duct temperatures. Power output or efficiency drop when detuned from the optimal. Thus, the duct temperatures are anchored to the coolant temperature, and the TAC is designed to run at a specific coolant temperature. For the TAC applications considered to date, this has not been a limitation.

7 Conclusions

The Etalim TAC is production-ready with a bottom-up costing study indicating a cost of $2/W at production volumes of 5000 / year. It is very competitive efficiency-wise with similar output power internal combustion engines and Stirling engines. The fault-free cumulative 8000-hour runtime reported here should go some way to substantiating our claims that the TAC is exceptionally reliable and requires only minimal maintenance. This engine is now a production-ready genset ideally suited for commercial deployment in various applications, including remote power, CHP, and waste heat recovery.

References

1. T. W. Steiner, G. D. S. Archibald, "A high pressure and high frequency diaphragm engine: Comparison of measured results with thermoacoustic predictions," Appl. Energy **114** (2014) 709-716.
2. T. Steiner, B. De Chardon, "Evolution of a diaphragm beta Stirling engine into a displacer-less thermoacoustic design," *Proceedings of the 17th International Stirling Engine Conference*, Northumbria University Newcastle UK, (2016), pp. 253-262.
3. R. S. Wakeland, "Use of electrodynamic drivers in thermoacoustic refrigerators," J. Acoust. Soc. Am. **107**, 827–832 (2000).
4. T. W. Steiner, K. B. Antonelli, G. D. S. Archibald, B. De Chardon, K. T. Gottfried, M. Malekian, P. Kostka, "A high frequency, power, and efficiency diaphragm acoustic-to-electric transducer for thermoacoustic engines and refrigerators," J. Acoust. Soc. Am. **149** (2021) 948-959. doi:https://doi.org/10.1121/10.0003495.
5. M. E. H. Tijani, S. Spoelstra, A hot air driven thermoacoustic-Stirling engine, Appl. Therm. Eng. **61** (2013) 866-870.
6. T. Bi, Z. Wu, L. Zhang, G. Yu, E. Luo, W. Dai, Development of a 5 kW traveling-wave thermoacoustic electric generator, Appl. Energy **185** (2017) 1355-1361.
7. C. Iniesta, J. L. Olazagoitia, J. Vinolas, J. Aranceta, "Review of traveling-wave thermoacoustic electric-generator technology," J. Power and Energy **232(7)** (2018) 940-957. doi:https://doi.org/10.1177/0957650918760627.
8. B. Medard de Chardon, T. W. Steiner, "Apparatus for performing energy transformation between thermal energy and acoustic energy," US patent 10,823,110 (2020).
9. T. W. Steiner, M. P. Hoy, G. D. S. Archibald, K. T. Gottfried, T. Kanemaru, B. Medard de Chardon, “Apparatus and system for exchanging heat with a fluid,” US patent 10,890,385 (2021).
10. T. W. Steiner, G. D. S. Archibald, T. J. Henthorne, M. P. Hoy, T. Kanemaru, "Thermal regenerator apparatus," US provisional patent application 62825592 (2019).
11. G. W. Swift, *Thermoacoustics A Unifying Perspective for Some Engines and Refrigerators*, 2nd Edition, ASA Press/Springer, Cham, Switzerland, (2017).
12. B. Ward, J. Clark, G. Swift, *DeltaEC users guide,* (2019) www.lanl.gov/thermoacoustics
13. J. R. Olson, G. W. Swift, "Acoustic streaming in pulse tube refrigerators: tapered pulse tubes," Cryogenics **37** (1997) 769-776.
14. M. A. G. Timmer, K. de Blok, and T. H. van der Meer, "Review on the conversion of thermoacoustic power into electricity," J. Acoust. Soc. Am. **143**, 841–857 (2018).
15. T. W. Steiner, M. Hoy, K. B. Antonelli, M. Malekian, G. D. S. Archibald, T. Kanemaru, W. Aitchison, B. De Chardon, K. T. Gottfried, M. Elferink, T. Henthorne, B. O'Rourke, and P. Kostka, "High-efficiency natural gas fired 1 kWe thermoacoustic engine," Accepted for publication, Appl. Therm. Eng., (2021). doi:https://doi.org/10.1016/j.applthermaleng.2021.117548
16. M. Raefsky, "Fatigue properties of 17-4 PH and 15-5 PH steel in the H-900 and H-1050 condition" (1968), https://apps.dtic.mil/dtic/tr/fulltext/u2/691794.pdf, Boeing Vertol Co. Philadelphia PA.

17. C. Bathias, P. C. Paris, *Gigacycle Fatigue in Mechanical Practice*, Marcel Dekker New York, (2005)

18. M. Elferink, T. Steiner, "Thermoacoustic waste heat recovery engine. Comparison of simulation and experiment," Proc. Mtgs. Acoust. 35 (2018) 955 065002. doi:https://doi.org/10.1121/2.0000978.